

# Quantum trajectories for time-binned data and their closeness to fully conditioned quantum trajectories

Nattaphong Wonglakhon,<sup>1</sup> Areeya Chantasri,<sup>1,2</sup> and Howard M. Wiseman<sup>1</sup>

<sup>1</sup>Centre for Quantum Computation and Communication Technology (Australian Research Council),  
Quantum and Advanced Technologies Research Institute,

Griffith University, Yarragba Country, Brisbane, Queensland 4111, Australia

<sup>2</sup>Optical and Quantum Physics Laboratory, Department of Physics,  
Faculty of Science, Mahidol University, Bangkok 10400, Thailand

(Dated: January 19, 2026)

Quantum trajectories are dynamical equations for quantum states conditioned on the results of a time-continuous measurement, such as a continuous-in-time current  $\vec{y}_t$ . Recently there has been renewed interest in dynamical maps for quantum trajectories with time-intervals of finite size  $\Delta t$ . Guilmartin *et al.* (unpublished) derived such a dynamical map for the (experimentally relevant) case where only the average current  $I_t$  over each interval is available. Surprisingly, this binned data still generates a conditioned state  $\rho_{\vec{y}_t}$  that is almost pure (for efficient measurements), with an impurity scaling as  $(\Delta t)^3$ . We show that, nevertheless, the typical distance of  $\rho_{\vec{y}_t}$  from  $\hat{\psi}_{F;\vec{y}_t}$  — the projector for the pure state conditioned on the full current — is as large as  $(\Delta t)^{3/2}$ . We introduce another finite-interval dynamical map (“ $\Phi$ -map”), which requires only one additional real statistic,  $\phi_t$ , of the current in the interval, that gives a conditioned state  $\hat{\psi}_{\Phi}$  which is only  $(\Delta t)^2$ -distant from  $\hat{\psi}_{F;\vec{y}_t}$ . We numerically verify these scalings of the error (distance from the true states) for these two maps, as well as for the lowest-order (Itô) map and two other higher-order maps. Our results show that, for a generic system, if the statistic  $\phi_t$  can be extracted from experiment along with  $I_t$ , then the  $\Phi$ -map gives a smaller error than any other.

## I. INTRODUCTION

Continuous quantum measurement [1–5] has been the object of sustained attention for decades, especially in quantum optics and, more recently, superconducting circuit experiments [6–15]. Such continuous measurements give rise to quantum state evolutions that are stochastic by nature, conditioned on measurement records, known as a *quantum trajectory* or *quantum state filtering* [16–18]. In practice, measurement records are acquired with a finite time resolution,  $\Delta t$ , yielding a *coarse-grained* measurement record or *time-binned current*  $I_t \propto \int_t^{t+\Delta t} y_s ds$ . Standard theoretical descriptions, however, are based on stochastic Schrödinger equations (SSEs) or, more generally, stochastic master equations (SMEs) [19, 20], both of which assume an infinitesimal time step. Consequently, quantum trajectories conditioned on coarse-grained currents  $I_t$  can exhibit significant deviations from the true underlying state evolution.

Several approaches have been proposed to propagate quantum trajectories over finite intervals by means of maps [21–25]. Our recent work [24] provided an extensive analysis of existing dynamical maps, and introduced a new one with superior properties. Nevertheless, it was only in Ref. [25] that a map was introduced that can be calculated (numerically) for arbitrary  $\Delta t$  and that describes quantum evolution conditioned solely on  $I_t$  by minimizing the mean trace-squared error (MTrSE) between the “*robinet*” state estimate [26]  $\rho_{\vec{y}_t}$  given the current  $I_t$ , and the quantum state  $\hat{\psi}_{F;\vec{y}_t}$  (which in this paper we take to be pure) conditioned on the full record,  $\vec{y}_t$  in each bin. This state,  $\rho_{\vec{y}_t}$ , is mixed, even for efficient measurements, because the binning process  $\vec{y}_t \rightarrow I_t$  throws away information. However, Ref. [25] also give an analytic expansion for their map up to  $(\Delta t)^{5/2}$ , and to this order it generates a state that is pure, so we write it  $\hat{\psi}_{\vec{y}_t}$ .

From the fact that the state conditioned on  $I_t$  is pure to order  $(\Delta t)^{5/2}$  one might think that the distance of  $\rho_{\vec{y}_t}$  from the fully conditioned state  $\hat{\psi}_{F;\vec{y}_t}$  would typically be even higher order than  $(\Delta t)^{5/2}$ . That is not the case, however; the distance is actually typically of order  $(\Delta t)^{3/2}$ , as depicted in Fig. 1(a). This raises the question: can we get a better estimate of  $\hat{\psi}_{F;\vec{y}_t}$ , perhaps using an expansion only to order  $(\Delta t)^{3/2}$ , if we adopt a different binning process? Here we answer that in the affirmative. Instead of binning the current  $\vec{y}_t \rightarrow I_t$ , its scaled mean in each time interval of duration  $\Delta t$ , we consider a binning process with two outputs:

$$\vec{y}_t \rightarrow \{I_t, \phi_t\} \quad (1)$$

where  $\phi_t \propto \int_t^{t+\Delta t} y_s [s - (t + \Delta t/2)] ds$ . This allows us to introduce what we call a *nearly exact map* ( $\Phi$ -map), an expansion to order  $(\Delta t)^{3/2}$  of the map of the fully conditioned state,  $\hat{\psi}_{F;\vec{y}_t}$ , which uses both  $I_t$  and  $\phi_t$ . We then show that this  $\Phi$ -map gives a state,  $\hat{\psi}_{\Phi}$ , that deviates from  $\hat{\psi}_{F;\vec{y}_t}$  only at order  $(\Delta t)^2$ , as illustrated by Fig. 1(b). Moreover, this  $\Phi$ -map has fewer terms than the robinet method, even when the latter is truncated at order  $(\Delta t)^2$ .

We analytically compare the exact (fully conditioned) state,  $\hat{\psi}_{F;\vec{y}_t}$ , to the “nearly exact” state,  $\hat{\psi}_{\Phi}$ , and to the robinet state,  $\hat{\psi}_{\vec{y}_t}$ , and states evolved by other discrete-time maps that have been proposed in the past, e.g., Itô [17], Rouchon-Ralph [21], Guevara-Wiseman, [22] and Wonglakhon *et al.* [24]. We find that quantum states obtained from all existing higher-order maps conditioned solely on  $I_t$  typically deviate from the fully conditioned state by an amount of order  $(\Delta t)^{3/2}$ . However, the size of the deviation depends on the details of the dynamics and the measurement. For example, the robinet method provides an exact map under the conditions of a quantum non-demolition (QND) measurement where the the observed oper-

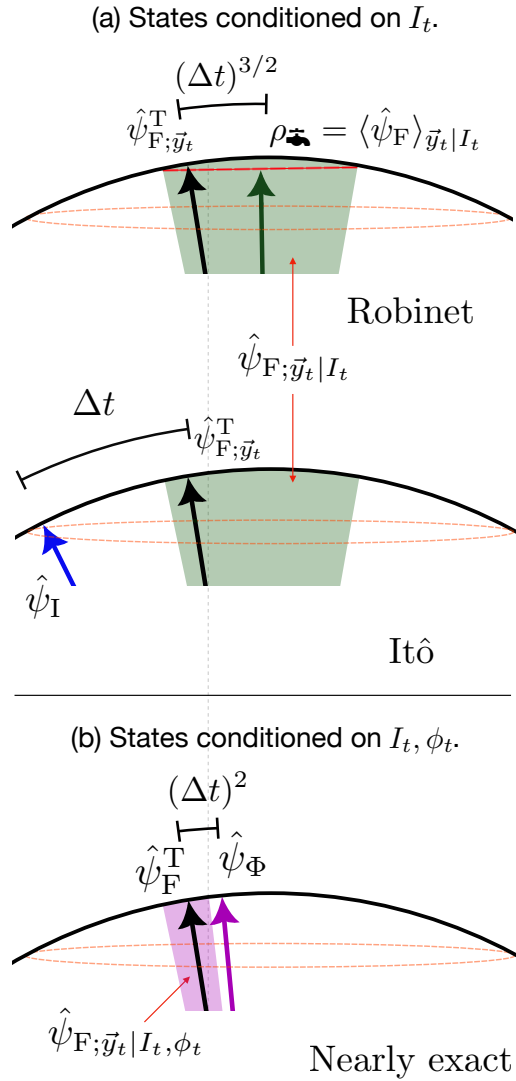


FIG. 1. **Bloch representation of pure-state estimates conditioned on different types of records.** The hypothetical true state,  $\hat{\psi}_{F;\vec{y}_t}^T$ , is represented by the fixed black arrows. **(a)** Quantum states conditioned only on  $I_t$ . The possible states conditioned on  $I_t$ ,  $\hat{\psi}_{F;\vec{y}_t|I_t}$ , are indicated by the light-green shaded area. The robinet state  $\rho_{\text{Robinet}}$ , represented by the green arrow, typically lies at a distance of order  $(\Delta t)^{3/2}$  from  $\hat{\psi}_{F;\vec{y}_t}^T$ . The crudest estimate,  $\hat{\psi}_I$  (Itô), is denoted by the blue arrow with a distance of order  $\Delta t$ . **(b)** Quantum states conditioned on both  $I_t$  and  $\phi_t$ . The possible states conditioned on  $\{I_t, \phi_t\}$ ,  $\hat{\psi}_{F;\vec{y}_t|I_t, \phi_t}$ , are indicated by the light-magenta shaded area. The nearly exact state  $\hat{\psi}_\Phi$  (magenta arrow) achieves a typical distance of order  $(\Delta t)^2$  from  $\hat{\psi}_{F;\vec{y}_t}^T$ .

ator  $\hat{c}$  is *normal*, so the distance would be limited only by the degree of expansion or other approximation method. We identify several such special cases relevant to the various maps that have been proposed, and verify their performance through numerical simulations.

By the above methodology, we confirm that the  $\Phi$ -map, giving a deviation of order  $(\Delta t)^2$  from the fully conditioned state

$\hat{\psi}_{F;\vec{y}_t}$ , is the best available higher-order map, in general, if one has access to  $\phi_t$  as well as  $I_t$ . This is so whether one is considering an actual (or simulated) experiment with the option of creating a binned record including  $\phi_t$  as well as  $I_t$  from raw data  $y_t$ , or whether one is creating a theoretical dual record  $\{I_t, \phi_t\}$  for the purpose of simulating an experiment entirely using a finite (but small) time step  $\Delta t$ .

The remainder of this paper is organized as follows. In Sec. II, we derive the fully conditioned map from the system–bath coupling formalism and review existing approaches. The nearly exact map and the corresponding statistical properties of the measurement records  $I_t$  and  $\phi_t$  are also introduced. Section III analyzes the errors associated with each existing method for quantum trajectory estimation and examines five special measurement cases and their corresponding error magnitudes. Section IV presents numerical simulations and analyzes of these five measurement scenarios. Finally, we summarize our findings and conclude in Sec. V.

## II. DYNAMICAL MAPS FOR QUANTUM TRAJECTORY SIMULATIONS

Although standard theoretical tools such as SSEs and SMEs are commonly employed for simulating quantum trajectories, these methods generally violate the condition of complete positivity (CP) under a finite time  $\Delta t$  assumption [24]. Alternative approaches based on Kraus operators (or *measurement operators*) have been developed, which inherently preserve the CP property [17, 21, 22, 24]. In this work, we therefore focus on the Kraus operator formalism.

In this section, we first derive the fully conditioned dynamical map from the system–bath interaction formalism in Sec. II A. The fully conditioned state serves as the foundation for constructing various dynamical maps, including the simplest form of Itô map and some other higher-order maps. Then, we review the existing higher-order measurement operators in the literature in Sec. II B. Lastly, in Sec. II C, we derive the nearly exact map which is one of the main results in this work.

### A. Fully conditioned dynamical map

To construct the fully conditioned state, let us recall a quantum system undergoing a time-continuous measurement, yielding a continuous result  $\vec{y}_t$  with white noise, as considered in Ref. [24]. We will use quantum optics terminology in referring to this as a homodyne measurement and current [17] but note that the same description applies in some non-optical contexts [7, 27]. As is standard, we model this by assuming the quantum system is coupled to a Markovian bosonic field. Given an infinitesimal time resolution  $dt$ , the measurement record  $y_s$  is collected from time  $t = s$  to  $t = s + dt$  through homodyne detection. This leads to a Kraus operator defined as

$$\hat{K}(y_t) = \langle y_t | \hat{U}_{t+dt,t} | 0 \rangle, \quad (2)$$

where the unitary operator in the rotating-wave approximation taking the form

$$\hat{U}_{t+\Delta t, t} = \exp[-i\hat{H}dt + \hat{c}d\hat{B}_t^\dagger - \hat{c}^\dagger d\hat{B}_t]. \quad (3)$$

The Hamiltonian  $\hat{H}$  is the system Hamiltonian in the interaction frame and  $d\hat{B}_t$  is the bath excitation operator satisfying  $[d\hat{B}_t, d\hat{B}_t^\dagger] = dt$  [17]. The bath is initially in the vacuum state  $|0\rangle$ , while  $|y_s\rangle$  represents the post-measurement state of the bath projected onto an eigenstate of the  $\hat{Q}_t$  quadrature operator,  $\hat{Q}_t|y_t\rangle = dt y_t |y_t\rangle$ , with  $\hat{Q}_t = d\hat{B}_t + d\hat{B}_t^\dagger$  [17, 24].

To consider a finite-time  $\Delta t$  evolution, we compute a product of  $m = \Delta t/dt$  Kraus operators, leading to the fully conditioned dynamical map given by

$$\begin{aligned} \hat{K}(\vec{y}_t) &= \lim_{m \rightarrow \infty} \hat{K}(y_{t+(m-1)\Delta t}) \cdots \hat{K}(y_t) \\ &= \lim_{m \rightarrow \infty} \prod_{s=t}^{t+(m-1)\Delta t} \langle y_s | \hat{U}_{s+\Delta t, s} | 0 \rangle, \end{aligned} \quad (4)$$

and the fully conditioned state reads

$$|\psi_{F;\vec{y}_t}(t + \Delta t)\rangle = \frac{\hat{K}(\vec{y}_t)|\psi(t)\rangle}{\sqrt{\wp_{\vec{y}_t}}}. \quad (5)$$

Here, we define a set of measurement records for each binning in a vector notation:  $\vec{y}_t = (y_t, \dots, y_{t+(m-1)\Delta t})^T$  and the normalization factor  $\wp_{\vec{y}_t} = \langle \psi_F(t) | \hat{K}^\dagger(\vec{y}_t) \hat{K}(\vec{y}_t) | \psi_F(t) \rangle$ . We refer to the quantum state  $|\psi_{F;\vec{y}_t}\rangle$  as a fully conditioned state because no measurement records are discarded. However, the exponential function in  $\hat{K}(\vec{y}_t)$  is, in general, difficult or impossible to analytically evaluate, and approximations are thus needed for a solvable analysis.

For the analysis below, it is useful to introduce the following notation for the expression of a pure state [e.g., in Eq. (5)] as a projector:

$$\hat{\psi}_A(t) \equiv |\psi_A(t)\rangle\langle\psi_A(t)|. \quad (6)$$

This allows us to accommodate general scenarios, especially those with a mixed state (in principle), such as  $\rho_{\vec{y}_t}$ .

## B. Existing dynamical maps

We start with approaches existing in the literature. Assuming  $\hat{H} = 0$  for now for simplicity, the simplest method is the Itô measurement operator  $\hat{M}_I$  [17]. It has been shown that the Itô operator can be derived by approximating  $\hat{U}_{t+\Delta t, t}$  in Eq. (2) to the lowest order in  $dt$  and using the *Itô's rule* [24]. By projecting to homodyne eigenstates, the resulted map is given by:

$$\hat{M}_I(I_t) = \hat{1} + I_t \hat{c}(\Delta t)^{1/2} - \frac{1}{2} \hat{c}^\dagger \hat{c} \Delta t, \quad (7)$$

where the dimensionless time-binned record  $I_t$  is defined via the coarse-grained records  $Y_t$  as

$$I_t \equiv (\Delta t)^{1/2} Y_t, \quad (8)$$

$$Y_t = \frac{1}{\Delta t} \int_t^{t+\Delta t} y_s ds. \quad (9)$$

The dimensionless variable makes the order of  $\Delta t$  explicit, which is particularly useful when comparing maps order by order, and it is also consistent with Ref. [25]. Here, their *ostensible probabilities* [17] are given by

$$\wp_{\text{ost}}(Y_t) = \sqrt{\frac{\Delta t}{2\pi}} \exp(-Y_t^2 \Delta t/2), \quad (10)$$

$$\wp_{\text{ost}}(I_t) = \frac{1}{\sqrt{2\pi}} \exp(-I_t^2/2), \quad (11)$$

from which one can define the Kraus form via  $\hat{K}_I(I_t) = \sqrt{\wp_{\text{ost}}(I_t)} \hat{M}_I(I_t)$ , which obeys the completeness condition

$$\int dI_t \hat{K}_I^\dagger(I_t) \hat{K}_I(I_t) = \hat{1} \quad (12)$$

with an error  $O[(\Delta t)^2]$ , while higher-order maps will obey this condition with errors of higher-order in  $\Delta t$ . Note that, in our analysis of the quantum state evolution following Eq. (5), the ostensible probability gets canceled out. Thus, we will henceforth only consider the unnormalized form  $\hat{M}$ , and refer it as *the* measurement operator.

The Itô map can easily cause errors in simulation as  $\Delta t$  is finite. Because of this, a higher-order map [Rouchon and Ralph [21]], was proposed, using the Euler-Milstein stochastic simulation method [21, 28]. They introduced a stochastic correction term from Itô map, which gives

$$\hat{M}_R(I_t) = \hat{M}_I(I_t) + \frac{1}{2} \hat{c}^2 (I_t^2 - 1) \Delta t \quad (13)$$

for stronger convergent of stochastic terms. Recent work by the current authors [Wonglakhon *et al.* [24]] showed that this can also be derived from the system-bath coupling formalism similar to the Itô map but without invoking the Itô rule. However, Ref. [24] also showed that the above two methods fail to unraveling Lindblad master equation [29, 30] to order of  $(\Delta t)^2$ . Ref. [24] thus proposed correction terms to the Rouchon-Ralph map, giving

$$\hat{M}_W(I_t) = \hat{M}_R(I_t) - \frac{I_t}{4} (\Delta t)^{3/2} \{ \hat{c}, \hat{c}^\dagger \hat{c} \} + \frac{1}{8} (\Delta t)^2 (\hat{c}^\dagger \hat{c})^2, \quad (14)$$

which is sufficient to produce Lindblad evolution with accuracy to  $O(\Delta t^2)$  for the ensemble average evolution (i.e., the Lindblad evolution).

Lastly, very recent work by Guilmartin *et al.* [25] has introduced a map to describe quantum evolution conditioned on time-binned currents  $I_t$ , named *robinet*. They present a dynamical map  $\mathcal{K}_{\vec{y}_t}$  for the density operator  $\rho$ . This is designed to produce a state  $\rho_{\vec{y}_t} = \arg \min \bar{\sigma}_{I_t}^2(\rho)$ , where  $\bar{\sigma}_{I_t}^2(\rho)$  is the MTrSE with the fully conditioned state  $\hat{\psi}_{F;\vec{y}_t}$ , given that only the time-binned current  $I_t$  is known:

$$\bar{\sigma}_{I_t}^2(\rho) = \langle \text{Tr}[(\rho - \hat{\psi}_{F;\vec{y}_t})^2] \rangle_{\vec{y}_t|I_t}. \quad (15)$$

Here the notation  $\langle \bullet \rangle_{\vec{y}_t|I_t}$  means  $\int d\vec{y}_t \wp(\vec{y}_t|I_t) \bullet$ , and  $\wp(\vec{y}_t|I_t)$  is the probability distribution of  $\vec{y}_t$  that gives  $I_t$ . From the

properties of the MTrSE, the action of  $\mathcal{K}_{\text{sc}}$  corresponds to taking the conditional average over all possible measurement records  $\vec{y}_t$  that yield the same  $I_t$ , i.e.,

$$\rho_{\text{sc}} = \mathcal{K}_{\text{sc}} \hat{\psi}(t) = \langle \hat{\psi}_{\text{F};\vec{y}_t}(t + \Delta t) \rangle_{\vec{y}_t|I_t}. \quad (16)$$

This results in a mixed state, in principle. However, we can consistently express their map expansion to  $O[(\Delta t)^2]$  via the measurement operator form as

$$\mathcal{K}_{\text{sc}} = \varphi_{\text{ost}}(I_t) \hat{M}_{\text{sc}}(I_t) \bullet \hat{M}_{\text{sc}}^\dagger(I_t) + O[(\Delta t)^{5/2}], \quad (17)$$

and the measurement operator reads:

$$\begin{aligned} \hat{M}_{\text{sc}}(I_t) &= \hat{M}_{\text{W}}(I_t) \\ &+ \frac{(\Delta t)^{3/2}}{6} (I_t^3 - 3I_t) \hat{c}^3 + \frac{(\Delta t)^2}{12} \left[ \frac{1}{2} (I_t^4 - 6I_t + 3) \hat{c}^4 \right. \\ &\quad \left. - (I_t^2 - 1) (\hat{c}^\dagger \hat{c}^3 + \hat{c} \hat{c}^\dagger \hat{c}^2 + \hat{c}^2 \hat{c}^\dagger \hat{c}) \right] \end{aligned} \quad (18)$$

with stochastic terms to  $O[(\Delta t)^2]$ . That is, to order  $(\Delta t)^2$ ,  $\mathcal{K}_{\text{sc}}$  is a purity-preserving map. We note that in the expression (18) we keep only terms to  $O[(\Delta t)^2]$ , so it differs from the operator as given in Ref. [25], which includes terms to  $O[(\Delta t)^{5/2}]$ . This is because truncating at  $(\Delta t)^2$  is sufficient to show our results as we will present in Sec. III. Notice also that all of the terms in Eq. (18) not in  $\hat{M}_{\text{W}}$  are stochastic (they involve the current). From the properties of Eq. (11), it is not difficult to see that they do not contribute to the Lindblad evolution up to order  $O[(\Delta t)^2]$ , as they average to zero. This confirms that  $\hat{M}_{\text{W}}(I_t)$  alone is sufficient to reproduce the Lindblad evolution correctly to  $O[(\Delta t)^2]$ .

In Ref. [24] we considered another higher-order method, proposed by Guevara and Wiseman [22]. We omit it from our analysis here because, although that approach satisfies the completeness condition up to order  $(\Delta t)^2$  Eq. (11), it yields a quantum state evolution whose accuracy is no better than that of the Itô method [24].

As stated in the Introduction, the quantum state conditioned solely on the current  $I_t$  typically suffers from errors arising from the loss of information during the time-binning process. Consequently, all of the maps introduced above generate quantum trajectories with only limited accuracy. In later sections, we show that the *typical* error distances scale as  $O[(\Delta t)^{3/2}]$  for all methods. To establish this result, we require a solvable higher-order reference state via the nearly exact map, which we derive below.

### C. Nearly exact map ( $\Phi$ -map)

In this section, we derive the nearly exact measurement operator starting from the system-bath Hamiltonian formalism. To this end, we revisit the operator  $\hat{H}$  in our derivation. Let us recall the operator  $\hat{K}(y_s)$  for an infinitesimal time interval  $dt$ . With the same treatment as in Ref. [24], but truncating Eq. (3) to order of  $(dt)^{3/2}$ , Eq. (2) can be written as

$$\hat{K}(y_s) = \langle y_s | \hat{U}_{s+dt,s} | 0 \rangle \equiv \hat{K}_{3/2}(y_s) + O[(dt)^2], \quad (19)$$

where we add the subscript ‘3/2’ to denote the truncation order. By expressing in the measurement operator form,  $\sqrt{\varphi_{\text{ost}}(y_s)} \hat{M}_{3/2}(y_s)$ , we obtain the approximated infinitesimal operator given by

$$\begin{aligned} \hat{M}_{3/2}(y_s) &= \hat{1} + y_s \hat{c} dt - \left( \frac{1}{2} \hat{c}^\dagger \hat{c} + i \hat{H} \right) dt + \frac{1}{2} \hat{c}^2 (y_s^2 dt - 1) dt \\ &+ \frac{1}{6} y_s \left[ \hat{c}^3 (y_s^2 dt - 3) - 2 \hat{c}^\dagger \hat{c}^2 - \hat{c} \hat{c}^\dagger \hat{c} - 3 \{ i \hat{H}, \hat{c} \} \right] dt^2. \end{aligned} \quad (20)$$

Here, the ostensible probability for  $y_s$  is given by a Gaussian function:  $\varphi_{\text{ost}}(y_s) = \sqrt{dt/(2\pi)} \exp(-y_s^2 dt/2)$ . Again, we construct the nearly exact map for the discretized interval via the product of  $m = \Delta t/dt$  operators:

$$\lim_{m \rightarrow \infty} \hat{M}_{3/2}(y_{t+(m-1)dt}) \cdots \hat{M}_{3/2}(y_t). \quad (21)$$

We provide the full derivation for Eq. (21) in Appendix A and construct the nearly exact map, given by

$$\begin{aligned} \hat{M}_\Phi(I_t, \phi_t) &= \hat{1} + I_t (\Delta t)^{1/2} \hat{c} - \frac{\Delta t}{2} \left[ \hat{c}^\dagger \hat{c} - \hat{c}^2 (I_t^2 - 1) + i \hat{H} \right] \\ &- \frac{(\Delta t)^{3/2}}{2} \left( I_t \left\{ \hat{c}, i \hat{H} + \frac{1}{2} \hat{c}^\dagger \hat{c} \right\} + \frac{\phi_t}{\sqrt{3}} \left[ \hat{c}, i \hat{H} + \frac{1}{2} \hat{c}^\dagger \hat{c} \right] \right. \\ &\quad \left. - \frac{I_t^3 - 3I_t}{3} \hat{c}^3 \right) + \frac{(\Delta t)^2}{2} \left[ \left( \frac{1}{2} \hat{c}^\dagger \hat{c} \right)^2 - \hat{H}^2 \right], \end{aligned} \quad (22)$$

where we use the subscript  $\Phi$  to emphasize the dependence on an additional unitless record variable  $\phi_t$ , defined by

$$\phi_t \equiv 2\sqrt{3}(\Delta t)^{-3/2} Z_t, \quad (23)$$

$$Z_t \equiv \int_t^{t+\Delta t} ds y_s \left[ s - \left( t + \frac{\Delta t}{2} \right) \right]. \quad (24)$$

While the record  $I_t$  describes a time-averaged (equally coarse-grained) data, the record  $\phi_t$  involves a linearly varying weighting over the time interval. We find the ostensible distribution for  $\phi_t$  to be

$$\varphi_{\text{ost}}(\phi_t) = \frac{1}{\sqrt{2\pi}} e^{-\phi_t^2/2}, \quad (25)$$

which is also a Gaussian function. The two Gaussian variables  $I_t$  and  $\phi_t$  are independent, and have identical moments. For convenience we list the moments for  $X_t \in \{I_t, \phi_t\}$  that will be useful:

$$\mathbb{E}[X_t]_{X_t} = 0, \quad \mathbb{E}[X_t^2]_{X_t} = 1, \quad \mathbb{E}[X_t^4]_{X_t} = 3. \quad (26)$$

The derivation of the measurement operator above follows the same fashion as in Ref. [24]. The key difference is that Ref. [24] focuses only on the ensemble-averaged evolution up to order  $(\Delta t)^2$ . As a result, terms proportional to  $\hat{c}^3$  were omitted, since they do not contribute to the average evolution at this order, and terms involving  $Z_t$  were also neglected because  $Z_t$  has zero mean and contributes only at order  $(\Delta t)^3$ .

There are two important points to note from the measurement operator in Eq. (22). First, the presence of  $\phi_t$  relates

to non-QND measurement effects, arising from a non-zero commutator of the system's Hamiltonian and the observed operator, i.e.,  $[\hat{H}, \hat{c}] \neq 0$ , or from the operator  $\hat{c}$  itself being non-normal i.e.,  $[\hat{c}, \hat{c}^\dagger] \neq 0$ . Second, we emphasize that no information is discarded up to  $O[(\Delta t)^{3/2}]$  in  $\hat{M}_\Phi(I_t, \phi_t)$ , so the map's errors consequently appear at  $O[(\Delta t)^2]$ . Moreover, those errors are stochastic only; we include deterministic terms up to order  $(\Delta t)^2$ , which ensures that the completeness relation which replaces Eq. (12),

$$\int dI_t d\phi_t \hat{K}_\Phi^\dagger(I_t, \phi_t) \hat{K}_\Phi(I_t, \phi_t) = \hat{1}, \quad (27)$$

is obeyed with an error  $O[(\Delta t)^2]$  (not  $O[(\Delta t)^2]$ ), and similarly the Lindblad evolution.

For all maps presented, we summarize the differences of each existing method and the  $\Phi$ -map in Table I, by comparing terms in order in  $\Delta t$ , up to order of  $(\Delta t)^2$ . All methods share common terms only up to order  $(\Delta t)^{1/2}$ . Beyond this, additional correction terms appear. For instance, the term  $(I_t^2 - 1)\hat{c}^2\Delta t/2$  serves as the post-Itô correction for  $\hat{M}_R$ , while  $-I_t\{\hat{c}, \hat{c}^\dagger\hat{c}\}(\Delta t)^{3/2}/4 + (\hat{c}^\dagger\hat{c})^2(\Delta t)^2/8$  is the the post-Rouchon-Ralph correction for  $\hat{M}_W$ , and so on. For consistency, we set  $\hat{H} = 0$  in the  $\Phi$ -map to match the other cases where we made that simplification.

#### D. Dynamical maps via superoperators

We now give the  $\Phi$ -map for a more general scenario allowing for imperfect measurement and additional decoherence. For this, rather than a measurement operator we need a superoperator:

$$\begin{aligned} \mathcal{K}_\Phi \propto & \mathcal{I} + (\Delta t)^{1/2}I_t\mathcal{C} + \Delta t\left(\mathcal{L} + \frac{I_t^2 - 1}{2}\mathcal{C}^2\right) \\ & + \frac{(\Delta t)^{3/2}}{2}\left(I_t\{\{\mathcal{LC}\}\} + \frac{I_t^3 - 3I_t}{3}\mathcal{C}^3 - \frac{\phi_t}{\sqrt{3}}[\mathcal{LC}]\right) \\ & + O[(\Delta t)^2], \end{aligned} \quad (28)$$

where  $\mathcal{K}_\Phi$  is conditioned on the records  $I_t, \phi_t$ , and the ostensible probabilities for  $I_t$  and  $\phi_t$  are the same as before. Here  $\mathcal{C}[\bullet] = \sqrt{\eta}\hat{c}\bullet + \bullet\sqrt{\eta}\hat{c}^\dagger$  appears in the stochastic measurement terms, with a measurement efficiency  $\eta$ . The Liouvillian is defined as  $\mathcal{L}\bullet = -i[\hat{H}, \bullet] + \hat{c}\bullet\hat{c}^\dagger - \frac{1}{2}(\hat{c}^\dagger\hat{c}\bullet + \bullet\hat{c}^\dagger\hat{c}) + \mathcal{L}'\bullet$ , where  $\mathcal{L}'$  contains any other Lindblad terms arising from additional decoherence. Generalizing Ref. [25], we have used the notations:  $\{\{\mathcal{LC}\}\} \equiv \mathcal{LC} + \mathcal{C}\mathcal{L}$  and  $[\mathcal{LC}] \equiv \mathcal{LC} - \mathcal{C}\mathcal{L}$ . We stress that the superoperator  $\mathcal{K}_\Phi$  generates quantum trajectory accurately at  $O[(\Delta t)^{3/2}]$ . This allows us to determine the errors generated by existing maps. For instance, the robinet method differs from  $\Phi$ -map, by what we call the “error superoperator”, defined as

$$\mathcal{E}_\Phi \equiv \mathcal{K}_\Phi - \mathcal{K}_R = -\frac{\phi_t}{2\sqrt{3}}(\Delta t)^{3/2}[\mathcal{LC}] + O(\Delta t^2). \quad (29)$$

From this it is clear that  $\mathcal{E}_\Phi$  indeed captures the non-QND effects. This is why, as stated explicitly in Ref. [25], the robinet

method entails the purity loss with a subtle size of  $O[(\Delta t)^3]$  despite a unity measurement efficiency ( $\eta = 1$ ) and no additional decoherence ( $\mathcal{L}' = 0$ ). We can independently show this as follows. In the notation of Eq. (6), consider an initial pure state  $\hat{\psi}_0$  and the state  $\hat{\psi}_\Phi$  under the  $\Phi$ -map for an interval  $\Delta t$ , which is also pure. Then  $\hat{\psi}_\Phi = \rho_\Phi + \mathcal{E}_\Phi \hat{\psi}_0 + O[(\Delta t)^2]$ , and it follows that

$$\hat{\psi}_\Phi^2 = \rho_\Phi^2 + \rho_\Phi(\mathcal{E}_\Phi \hat{\psi}_0) + (\mathcal{E}_\Phi \hat{\psi}_0)\rho_\Phi + (\mathcal{E}_\Phi \hat{\psi}_0)^2 + O[(\Delta t)^4]. \quad (30)$$

By taking the ensemble average over  $\phi_t$  via the properties in Eqs. (26), this leads to

$$\mathbb{E}[\hat{\psi}_\Phi^2]_{\phi_t} = \rho_\Phi^2 + \frac{(\Delta t)^3}{12}([\mathcal{LC}]\rho_0)^2 + O[(\Delta t)^{7/2}]. \quad (31)$$

By taking the trace over the system, Eq. (31) is evaluated as  $\text{Tr}\{\mathbb{E}[\hat{\psi}_\Phi^2]_{\phi_t}\} = 1$  and leads to

$$\text{Tr}[\rho_\Phi^2] = 1 - \frac{(\Delta t)^3}{12}\text{Tr}[(\mathcal{LC})\rho_0]^2 + O[(\Delta t)^{7/2}], \quad (32)$$

with the subtle effect appearing in order  $(\Delta t)^3$ .

Turning to other existing maps, we derive the maps' superoperators in similar manner as above. Here, the Itô approach yields:  $\mathcal{K}_I \propto \mathcal{I} + (\Delta t)^{1/2}I_t\mathcal{C} + O(\Delta t)$ , which, as expected, is only correct to  $O[(\Delta t)^{1/2}]$ . For the Rouchon-Ralph approach, we can define the superoperator  $\mathcal{K}_R \propto \mathcal{I} + (\Delta t)^{1/2}I_t\mathcal{C} + \Delta t[\mathcal{L} + (I_t^2 - 1)\mathcal{C}^2/2]$ , which directly yields the second line in Eq. (28), and leads to the error, given by

$$\mathcal{E}_R = \mathcal{K}_\Phi - \mathcal{K}_R = O[(\Delta t)^{3/2}], \quad (33)$$

making it the simplest approach to produce quantum trajectories accurately to order  $\Delta t$ . We note that the map  $\mathcal{K}_R$  can also be found in Ref. [21]. Since the Rouchon-Ralph method is the simplest map that is correct at  $\Delta t$ , we shall use it in Sec. IV for approximately generating fully conditioned states  $\hat{\psi}_{F;\bar{y}_t}$  via an extremely small time increment. Lastly,  $\hat{M}_W$  results in  $\mathcal{K}_W \propto \mathcal{K}_R + I_t\{\{\mathcal{LC}\}\}(\Delta t)^{3/2}/2 + O[(\Delta t)^{3/2}]$  with an additional correction term from  $\mathcal{K}_R$ . Like both robinet and Rouchon-Ralph,  $\mathcal{E}_W = O[(\Delta t)^{3/2}]$ .

### III. STATE EVOLUTION AND THEIR ERRORS

In general, the errors of quantum state estimation depends on the amount of information available from the measurement record. That is, a quantum state that is fully conditioned on the entire measurement record  $\bar{y}_t$  yields the most accurate quantum state estimate. However, when some information is lost and only certain types of measurement records are available (e.g., the coarse-grained records like  $I_t$  and  $\phi_t$ ), the resulting estimation inevitably incurs errors. It follows that a quantum state conditioned only on the time-binned record  $I_t$  is generally less accurate than one conditioned on more information, such as both  $I_t$  and  $\phi_t$ .

Orders	All maps	$\hat{M}_{\Phi \cap \text{R} \cap \text{W} \cap \text{R}}$	$\hat{M}_{\Phi \cap \text{R} \cap \text{W}}$	$\hat{M}_{\Phi \cap \text{R}}$	$\hat{M}_{\Phi}$	$\hat{M}_{\Phi}$
$(\Delta t)^0$	$\hat{1}$					
$(\Delta t)^{1/2}$	$I_t \hat{c}$					
$\Delta t$	$-\frac{1}{2} \hat{c}^\dagger \hat{c}$	$\frac{1}{2} (I_t^2 - 1) \hat{c}^2$				
$(\Delta t)^{3/2}$			$-\frac{1}{4} I_t \{ \hat{c}, \hat{c}^\dagger \hat{c} \}$	$\frac{1}{6} (I_t^3 - 3I_t) \hat{c}^3$		$-\frac{1}{4\sqrt{3}} \phi_t [\hat{c}, \hat{c}^\dagger \hat{c}]$
$(\Delta t)^2$			$\frac{1}{8} (\hat{c}^\dagger \hat{c})^2$		$-\frac{1}{12} (I_t^2 - 1) (\hat{c}^\dagger \hat{c}^3 + \hat{c} \hat{c}^\dagger \hat{c}^2 + \hat{c}^2 \hat{c}^\dagger \hat{c})$ $+\frac{1}{24} (I_t^4 - 6I_t^2 + 3) \hat{c}^4$	

TABLE I. **Common and correction terms of maps:** The measurement operators are defined in Eqs. (7), (13), (14), (18) and (22) (setting  $\hat{H} = 0$  in the last case, for consistency). Notation:  $\hat{M}_{\text{A} \cap \text{B}} = \hat{M}_{\text{A}} \cap \hat{M}_{\text{B}}$  indicates the common terms of the considered methods.

In this section, we will explore these errors in quantum state evolution conditioned on records  $X_t \in \{I_t, \phi_t\}$ . For simplicity we consider the quantum state evolution for  $\hat{H} = 0$ , with only one decoherence channel  $\hat{c}$  (the measured one), and with unit efficiency measurement. Thus we can use the pure-state maps

$$|\psi_{\text{A}}(t + \Delta t)\rangle = \frac{\hat{M}_{\text{A}}(X_t)|\psi(t)\rangle}{\sqrt{\rho_{\text{A}}}}. \quad (34)$$

We conduct the error analysis via its projector form  $\hat{\psi}_{\text{A}}$ . We first evaluate the typical errors for an arbitrary  $\hat{c}$  of each method in Sec. III A and provide the error analysis for special cases in Sec. III B.

### A. Typical errors for an arbitrary measurement process

In this section, we consider the error for an arbitrary measurement process  $\hat{c}$ . It is natural to evaluate the errors by comparing each estimated state with the fully conditioned state  $\hat{\psi}_{\text{F};\bar{y}_t}$ . Here we consider the trace distance  $D$  as a metric, which corresponds to the trace absolute error (TrAE) when one of the states is the true state. Although the TrAE is not the measure used to define the optimality of quantum state estimates, we employ it because it is analytically convenient and allows direct comparison with the analytical results of our companion work [24]. Moreover, for the case of pure states (which is the case, or very nearly so, for all the estimates we consider),  $D_{\text{A},\text{B}} = \frac{1}{2} \text{Tr} [|\hat{\psi}_{\text{A}} - \hat{\psi}_{\text{B}}|] = \sqrt{1 - |\langle \psi_{\text{A}} | \psi_{\text{B}} \rangle|^2}$ , while the TrSE is  $\sigma_{\text{A},\text{B}}^2 = \text{Tr}[(\hat{\psi}_{\text{A}} - \hat{\psi}_{\text{B}})^2] = 2(1 - |\langle \psi_{\text{A}} | \psi_{\text{B}} \rangle|^2)$ . The two measures are thus simply related as  $2D^2 = \sigma^2$ , and therefore exhibit the same scaling behavior.

A challenge for calculating the error from the true state is that deriving  $\hat{\psi}_{\text{F};\bar{y}_t}$  in the general case is intractable. To overcome this, we instead use the  $\Phi$ -map in our analysis, as we have it explicitly. This works for the following reason. For any quantum states, the trace distance defined as  $D_{\text{A},\text{B}}$  satisfies the *triangle inequality* [31],

$$D_{\text{A},\text{B}} \leq D_{\text{A},\text{C}} + D_{\text{C},\text{B}}. \quad (35)$$

From Eq. (35), one can derive distances relating  $\hat{\psi}_{\text{A}}$ ,  $\hat{\psi}_{\text{F};\bar{y}_t}$ , and  $\hat{\psi}_{\Phi}$ , as  $D_{\text{A},\text{F}} \leq D_{\text{A},\Phi} + D_{\Phi,\text{F}}$  and  $D_{\text{A},\Phi} \leq D_{\text{A},\text{F}} + D_{\text{F},\Phi}$ . Using the fact that  $D_{\Phi,\text{F}} = D_{\text{F},\Phi}$ , we obtain

$$-D_{\Phi,\text{F}} \leq D_{\text{A},\text{F}} - D_{\text{A},\Phi} \leq D_{\Phi,\text{F}}, \quad (36)$$

which leads to  $|D_{\text{A},\text{F}} - D_{\text{A},\Phi}| \leq D_{\Phi,\text{F}}$ . Given that the  $\Phi$ -map produces a state whose distance from the fully conditioned state as claimed in Sec. II C is

$$D_{\Phi,\text{F}} = O[(\Delta t)^2], \quad (37)$$

Eq. (37) implies that

$$|D_{\text{A},\text{F}} - D_{\text{A},\Phi}| \leq O[(\Delta t)^2] \quad (38)$$

Hence, we can indirectly evaluate the errors of  $\hat{\psi}_{\text{A}}$  relative to  $\hat{\psi}_{\text{F};\bar{y}_t}$  via  $D_{\text{A},\Phi}$  as long as these errors are bigger than  $O[(\Delta t)^2]$ . As we will see below, this is always the case, in general.

Here, we expand the trace distance with respect to  $\Delta t$  using the Maclaurin expansion to evaluate  $D_{\text{A},\text{B}} = \text{Tr}[\hat{\psi}_{\text{A}} - \hat{\psi}_{\text{B}}]$  and find that the typical distances are:  $D_{\text{I},\Phi} = O(\Delta t)$  and  $D_{\text{A},\Phi} = O[(\Delta t)^{3/2}]$  for  $\text{A} \in \{\text{R}, \text{W}, \text{R}\}$ . These allow us to establish the typical errors of each method, which are given by

$$D_{\text{I},\text{F}} = O(\Delta t), \quad (39a)$$

$$\left. \begin{aligned} D_{\text{R},\text{F}} \\ D_{\text{W},\text{F}} \\ D_{\text{R}\text{R},\text{F}} \end{aligned} \right\} = O[(\Delta t)^{3/2}]. \quad (39b)$$

We note that although  $D_{\text{R},\text{F}}$ ,  $D_{\text{W},\text{F}}$ , and  $D_{\text{R}\text{R},\text{F}}$  have the same magnitude in  $O[(\Delta t)^{3/2}]$ , their prefactor scalings may differ. Moreover, the results in Eqs. (39) may change for some specific details of the measurement process  $\hat{c}$ , which we shall see in the next subsection.

We remind the reader that we use the pure state  $|\psi_{\text{A}}\rangle$  in our analysis as it is solvable, where  $\hat{\psi}_{\text{A}} = |\psi_{\text{A}}\rangle\langle\psi_{\text{A}}|$  via  $\hat{M}_{\text{A}}$  defined in Eq. (18). Here,  $\hat{\psi}_{\text{A}}$  is not equal to the mixed state  $\rho_{\text{A}}$  in Eq. (16), but they can be related by  $\rho_{\text{A}} = \hat{\psi}_{\text{A}} + O[(\Delta t)^{5/2}]$ . However, the typical error for  $\rho_{\text{A}}$  still reads  $\text{Tr}|\rho_{\text{A}} - \hat{\psi}_{\text{F}}| = O[(\Delta t)^{3/2}]$ , following Eq. (29).

To provide an intuitive picture of the errors of the results in Eqs. (39) and the  $\Phi$ -map, we consider the evolution of a pure state conditioned on the dual data  $I_t$  and  $\phi_t$ , as illustrated in Fig. 1. To see errors of a quantum state conditioned on  $\bar{y}_t \rightarrow \{I_t, \phi_t\}$ , we first define a “hypothetical true state”,  $\hat{\psi}_{F; \bar{y}_t}^T$ , conditioned on complete knowledge of measurement records  $y_t$ , represented by the black arrows. We use this extra superscript (T) to distinguish it from  $\hat{\psi}_{F; \bar{y}_t}$ , which we treat as a possible true state (conditioned on the full record  $\bar{y}_t$ ) having a probability distribution conditioned on the observer’s available record. That is,  $\hat{\psi}_{F; \bar{y}_t}^T$  corresponds to the actual realization of  $\bar{y}_t$  and is therefore fixed and independent of the observer’s information. The state  $\hat{\psi}_{F; \bar{y}_t}^T$  thus serves as a reference for pictorially indicating the typical size of the errors generated by different trajectory maps.

Fig. 1(a) shows the case where only the measurement record  $I_t$  is available,  $\bar{y}_t \rightarrow I_t$ . In this case, the robinet state  $\rho_{\text{R}}$ , represented by the green arrow, lies at the midpoint of the light-green shaded region, as it minimizes the MTrSE for quantum states conditioned on  $I_t$ . Explicitly, it is given by the ensemble average  $\rho_{\text{R}} = \langle \hat{\psi}_{F; \bar{y}_t}^T \rangle_{y_t|I_t}$ , and is hence a (very slightly) mixed state. The light-green shaded region represents the standard deviation  $\sigma_{\bar{y}_t|I_t}$  of the distribution of  $\hat{\psi}_{F; \bar{y}_t}^T$  when conditioned only on the record  $I_t$ . Here, the standard deviation is defined as the root MTrSE from  $\rho_{\text{R}}$ , and will scale in the same way as the trace distance  $D_{\text{R}, F}$ . Specifically, using Eq. (29) together with Eq. (38), we have  $\sigma_{\bar{y}_t|I_t} = O(D_{\text{R}, F}) = O[(\Delta t)^{3/2}]$ . This is both the size of the shaded region, and the typical distance of  $\rho_{\text{R}}$  from  $\hat{\psi}_{F; \bar{y}_t}^T$ , because  $\rho_{\text{R}}$  is an optimal estimate of  $\hat{\psi}_{F; \bar{y}_t}^T$ .

By contrast, for non-optimal estimates, the typical deviation is greater than the size of shaded region. At the most extreme,  $\hat{\psi}_I$  (blue arrow), the estimate from the Itô map, lies at a typical distance of order  $\Delta t$  from  $\hat{\psi}_{F; \bar{y}_t}^T$ , as determined by  $D_{I, F}$ . Other maps such as  $\hat{M}_R$  and  $\hat{M}_W$ , exhibit closer deviations of order  $(\Delta t)^{3/2}$  from  $\hat{\psi}_{F; \bar{y}_t}^T$  which are the same scaling as that of  $\rho_{\text{R}}$ , but larger.

In Fig. 1(b), additional information from  $\phi_t$  is available,  $\bar{y}_t \rightarrow \{I_t, \phi_t\}$ , and the corresponding possible state,  $\hat{\psi}_{F; \bar{y}_t|I_t, \phi_t}$ , shows a smaller uncertainty denoted by the light magenta region. The standard deviation for this scenario is conjectured to scale as  $O[(\Delta t)^{5/2}]$ , where one would require a “super  $\Phi$ -map” which is accurate to  $(\Delta t)^2$  to verify this. Crucially, even though the nearly exact map does not give an optimal estimate conditioned on  $\{I_t, \phi_t\}$ , the state  $\hat{\psi}_\Phi$  (magenta arrow) lies at a typical distance only of order  $(\Delta t)^2$  from  $\hat{\psi}_{F; \bar{y}_t}^T$ . This reflects the fact that it is a much more accurate estimate state, which is possible because it requires extracting twice as much information from the full record.

## B. Special cases

As Eqs. (39) provide typical error distances for an arbitrary operator  $\hat{c}$ ; however, there are special scenarios such that some maps may change their orders of error distances depending on

the properties of  $\hat{c}$ . We emphasize that we consider  $\hat{H} = 0$  case, so that  $[\hat{H}, \hat{c}] = 0$ . In this section, we again utilize the  $\Phi$ -map to evaluate the error distances for the special cases as follows.

*Case 1:  $\hat{c}^2 \propto \hat{1}$*

In this case,  $\hat{M}_I$  is enhanced relative to the general case because the Rouchon-Ralph correction term (proportional to  $\hat{c}^2$ ) commutes with other terms. As a result,  $D_{A, \Phi} = O[(\Delta t)^{3/2}]$ , for  $A \in \{I, R, W, \text{R}\}$ . Using Eq. (38), we can conclude the error distances for this case as

$$\left. \begin{array}{l} D_{I, F} \\ D_{R, F} \\ D_{W, F} \\ D_{\text{R}, F} \end{array} \right\} = O[(\Delta t)^{3/2}]. \quad (40)$$

A physical example of Case 1 is a qubit Pauli-measurement with  $\hat{c} \propto \hat{\sigma}_{x, y, z}$ , where the operators are defined in Appendix B. Notably, Ref. [24] has verified this error analysis analytically.

*Case 2:  $\hat{c}^2 = 0$*

This is actually a special case of Case 1, with the additional consequences that  $\hat{M}_I = \hat{M}_R$  and  $\hat{M}_W = \hat{M}_{\text{R}}$ . Following Case 1, the error distances read:

$$\left. \begin{array}{l} D_{I, F} = D_{R, F} \\ D_{W, F} = D_{\text{R}, F} \end{array} \right\} = O[(\Delta t)^{3/2}]. \quad (41)$$

The qubit fluorescence measurement is an example of Case 2, with  $\hat{c} \propto \frac{1}{2}(\hat{\sigma}_x - i\hat{\sigma}_y) = \hat{\sigma}_-$ . Again, Ref. [24] has also verified this analytically.

*Case 3:  $\hat{c}^3 = 0$*

In this case,  $\hat{M}_W = \hat{M}_{\text{R}} + O[(\Delta t)^2]$ . We find that  $D_{I, \Phi} = O(\Delta t)$ , while  $D_{A, \Phi} = O[(\Delta t)^{3/2}]$  for  $A \in \{R, W, \text{R}\}$ . Using Eq. (38), we hence have the error distances:

$$D_{I, F} = O(\Delta t), \quad (42a)$$

$$\left. \begin{array}{l} D_{R, F} \\ D_{W, F} \end{array} \right\} \simeq D_{\text{R}, F} = O[(\Delta t)^{3/2}]. \quad (42b)$$

Here the  $\simeq$  in Eq. (42b) means they are the same to leading order in  $\Delta t$ , but different at higher-order terms. As an example of Case 3, we can consider a spin-1 system with  $\hat{c} \propto (\hat{S}_x - i\hat{S}_y)/2 = \hat{S}_-$ . (We define the operator  $\hat{S}_{x, y, z}$  in Appendix B.) This choice does not fall under Case 1 or 4.

*Case 4:  $[\hat{c}, \hat{c}^\dagger] = 0$*

That is, Case 4 is where the operator  $\hat{c}$  is *normal*, i.e.,  $[\hat{c}, \hat{c}^\dagger] = 0$ . Since  $[\hat{H}, \hat{c}] = 0$  because we are taking  $\hat{H} = 0$ ,

this is the case of QND measurements. In this case, the robinet method provides an exact solution where the nontrivial coarse-grained record (e.g.,  $\phi_t$ ) makes no contribution, and the exact state evolution is conditioned solely on  $I_t$ . As  $\hat{M}_{\text{R}}$  is the expansion truncated at  $O[(\Delta t)^2]$ , we can directly determine

$$D_{\text{R}, \text{F}} = O[(\Delta t)^{5/2}]. \quad (43)$$

We also find that  $D_{\text{I}, \Phi} = O(\Delta t)$  and  $D_{\text{A}, \Phi} = O[(\Delta t)^{3/2}]$  for  $\text{A} \in \{\text{R}, \text{W}\}$ . Thus, the error distances read:

$$D_{\text{I}, \text{F}} = O(\Delta t), \quad (44\text{a})$$

$$\left. \begin{array}{l} D_{\text{R}, \text{F}} \\ D_{\text{W}, \text{F}} \end{array} \right\} = O[(\Delta t)^{3/2}], \quad (44\text{b})$$

$$D_{\text{A}, \text{F}} = O[(\Delta t)^{5/2}]. \quad (44\text{c})$$

Again, we remind the reader that  $\rho_{\text{R}}$  gives the exact evolution in this case, i.e.,  $|\rho_{\text{R}} - \hat{\psi}_{\text{F}, \hat{y}_t}| = 0$ , and the nonzero error in Eq. (44c) appears only because we have defined  $\hat{M}_{\text{R}}$  to be the robinet map truncated at  $O[(\Delta t)^2]$ . To give example for this case, we can take  $\hat{c} \propto \hat{\sigma}_{x,y,z}$  for a qubit system or  $\hat{c} \propto \hat{S}_{x,y,z}$  for spin-1 systems. We choose the latter in Sec. IV, as it as an example that does not also fall under Case 1.

#### Case 5: no condition

This case reflects the general scenario where the error distances are given by Eqs. (39). For example, we can take a lowering operator for a spin-3/2 system,  $\hat{L}_-$ , defined in Appendix B, which does not fall into any of the other Cases.

## IV. NUMERICAL SIMULATION

To verify the error distances provided in the preceding section, we conduct numerical simulations for five measurement examples to reflect the special cases. Again, we consider a single measured operator  $\hat{c}$  with  $\eta = 1$ . The settings for each case are stated as follows.

- Example 1: spin-1/2 (qubit) system,  $\hat{c} = \sqrt{\gamma/2}\hat{\sigma}_z$ ,  $|\psi(0)\rangle = |+x\rangle$ , defined in Appendix B, and this example demonstrates Case 1 and Case 5.
- Example 2: spin-1/2 system,  $\hat{c} = \sqrt{\gamma}\hat{\sigma}_-$  with the same initial state as Example 1, and this example demonstrates Case 2.
- Example 3: spin-1 system,  $\hat{c} = \sqrt{\gamma}\hat{S}_-$ ,  $|\psi(0)\rangle = |+x\rangle_1$ , defined in Appendix B, and this example demonstrates Case 3.
- Example 4: spin-3/2 system,  $\hat{c} = \sqrt{\gamma}\hat{L}_-$ ,  $|\psi(0)\rangle = |+x\rangle_{3/2}$ , defined in Appendix B, and this example demonstrates Case 4.

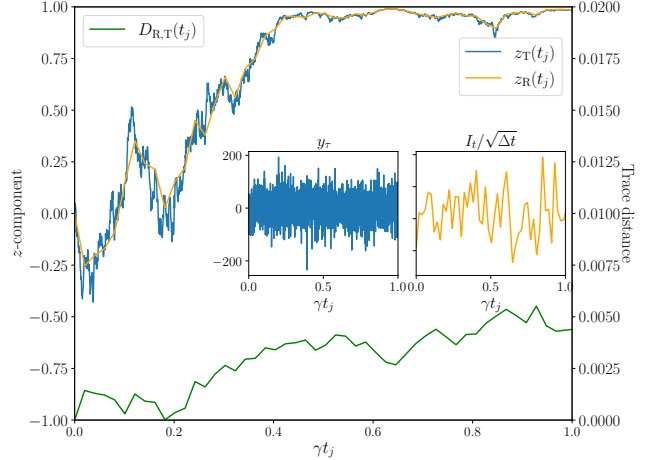


**FIG. 2. True and finite-time trajectories:** This example depicts the qubit  $z$ -measurement with  $\hat{c} = \sqrt{\gamma/2}\hat{\sigma}_z$ . The true record ( $y_\tau$ ) and its corresponding trajectory ( $z_T(t_j) = \text{Tr}[\hat{\sigma}_z \hat{\psi}_T(t_j)]$ ) are shown in the blue curves, while the coarse-grained record ( $I_t$ ) and its corresponding trajectory,  $z_R(t_j)$ , are denoted by the orange curves. The trajectories are simulated using  $\hat{M}_R(I_{t_j})$ . The green curve indicates the trace distance of the trajectory from the coarse-grained record comparing with the true one,  $D_{R,k}(t_j)$ . Parameters:  $\eta = 1$ , and  $\gamma = 1$ .

- Example 5: spin-1 system,  $\hat{c} = \sqrt{\gamma/2}\hat{S}_z$  with the same initial state as Example 3, and this example demonstrates Case 5.

We will present the simulation procedure for each special case in Sec. IV A and then analyze the numerical results in Sec. IV B.

### A. Simulation procedures

To make a fair comparison, we introduce a “true” quantum state as a benchmark for evaluating errors generated by the existing methods. We define our true trajectories generated by using an extremely small time resolution  $\delta t$ . This is to ensure that any higher-order errors associated with any methods used in generating the true trajectories vanish, i.e.,  $O[(\gamma\delta t)^n] \rightarrow 0$ , for a relevant coupling rate  $\gamma$ . In this work, we use  $\gamma\delta t = 10^{-4}$  for the true evolution and  $\gamma\Delta t = 10^{-2}$  for the finite  $\Delta t$  evolution (e.g., the  $\Delta t$  can be an experimentally relevant time scale).

Since true trajectories with  $\eta = 1$  should all be pure states, we can write the true state evolution conditioned on a “true” measurement record  $y_{t_j}$  at a time  $t_j$ :

$$|\psi_T(t_j + \delta t)\rangle = \frac{\hat{M}_R(y_{t_j})|\psi(t_j)\rangle}{\sqrt{\wp_T(y_{t_j})}}, \quad (45)$$

using the operator  $\hat{M}_R(y_{t_j})$  defined in Eq. (13) (replacing  $\Delta t$  with  $\delta t$  and  $I_t$  with  $(\delta t)^{1/2}y_t$ ) and the probability norm is defined as  $\wp_T(y_{t_j}) = \langle\psi_T(t_j)|\hat{M}_R^\dagger(y_{t_j})\hat{M}_R(y_{t_j})|\psi_T(t_j)\rangle$ . We

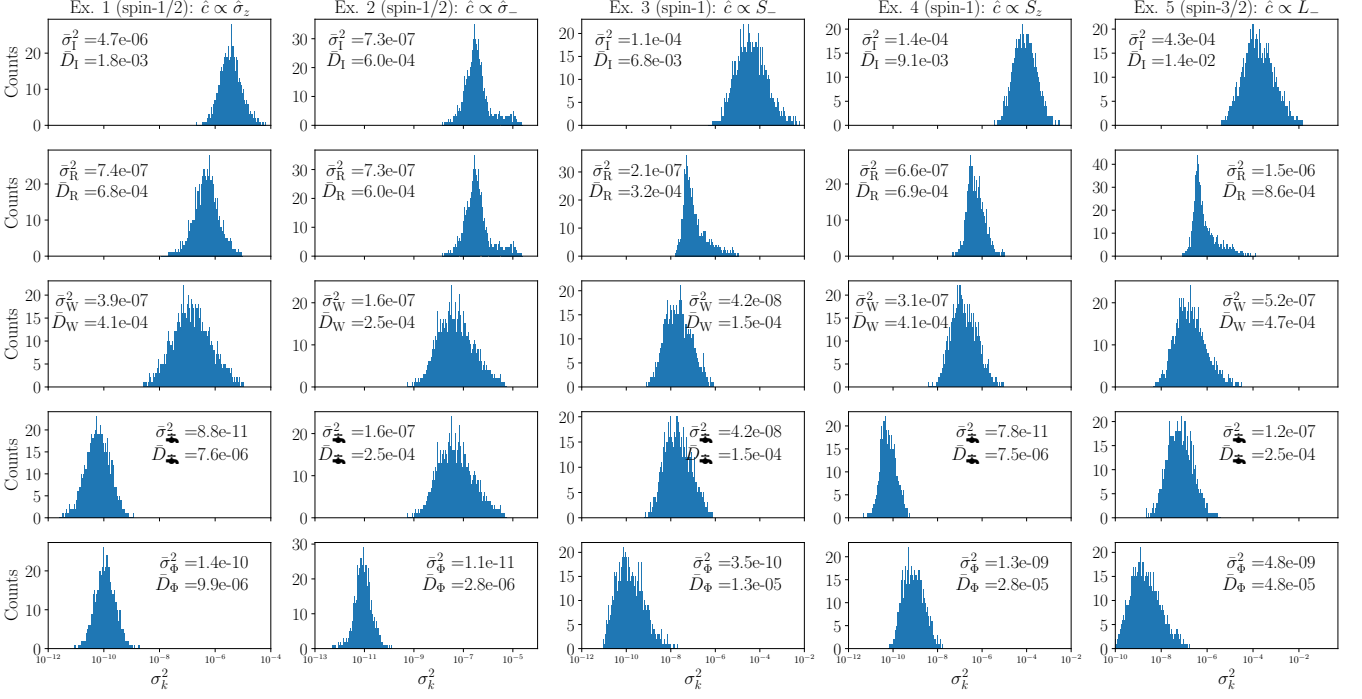


FIG. 3. **Time-average trace-squared errors:** the histograms show  $\sigma_{A;k}^2$  computed via Eq. (49) (log-scaled) of individual trajectories,  $|\psi_A\rangle$ , generated by each method comparing with the true state,  $|\psi_T\rangle$ , of five special quantum measurement examples. The MTrSEs ( $\bar{\sigma}_A^2$ ) and MTrAEs ( $\bar{D}_A$ ) for method A are reported in the plots. The subscript texts are A  $\in \{I, R, W, \Phi, \Psi\}$ , used to indicate the numerical results from the maps:  $\hat{M}_I$ ,  $\hat{M}_R$ ,  $\hat{M}_W$ ,  $\hat{M}_\Phi$ , and  $\hat{M}_\Psi$  ( $\Phi$ ), respectively. Parameters:  $\hat{H} = 0$ , and  $\gamma = 1$  for all cases.

note that the operator  $\hat{M}_R$  was chosen for the true trajectories because it is the simplest approach that ensures the state errors are in order of  $(\gamma\delta t)^{3/2} = O(10^{-6})$  as determined in Eq. (33). Given this, the true states are thus reliable for the finite  $\Delta t$  evolution with an accuracy of  $O(10^{-6})$  with the same scaling as  $O[(\gamma\Delta t)^3]$ . One could consider using the even simpler map  $\hat{M}_I$ , though it would lead to a typical error of  $(\gamma\delta t) = O(10^{-4})$ , which is not adequate for a reliable analysis, especially for maps with higher-order terms in  $O[(\Delta t)^2]$ . We remark that, in our numerical simulation, we choose  $\eta = 1$  which results in pure states for the trajectories for the sake of simplicity. One can easily extend to a mixed state evolution using density matrix formalisms.

*True evolution with  $\delta t$ :* At any time step  $t$  with a quantum state  $|\psi_T(t)\rangle$ , we construct a true measurement record by combining a deterministic and stochastic parts,

$$y_t\delta t = \mu_t\delta t + \delta W, \quad (46)$$

where the (state-dependent) deterministic component is given by:  $\mu_t = \langle\psi_T(t)|(\hat{c} + \hat{c}^\dagger)|\psi_T(t)\rangle$ , which depends on the observed operator  $\hat{c}$ . The stochastic component is described by a Wiener increment  $\delta W$ , generated with a Gaussian distribution with zero mean and  $\delta t$  variance. Given  $y_t$  in Eq. (46), the quantum state is then updated via Eq. (45) and then the process is repeated to obtain the true evolution for a fixed total time  $T$ .

*Finite-time evolution with  $\Delta t$ :* To simulate the finite  $\Delta t$  evolution, we start with computing the two coarse-grained

records by deriving Eqs. (8) and (23), which are now written in time-discrete forms as

$$I_{t_j} \frac{1}{\sqrt{\Delta t}} = \frac{1}{n} \sum_{\tau=t_j}^{t_j+(n-1)\delta t} y_\tau, \quad (47a)$$

$$\phi_{t_j} \frac{\Delta t^{3/2}}{2\sqrt{3}} = \delta t \sum_{\tau=t_j}^{t_j+(n-1)\delta t} y_\tau [(\tau - 1)\delta t - \Delta t/2], \quad (47b)$$

using  $y_\tau$  defined in Eq. (46). Here, we used  $n = \Delta t/\delta t = 100$  as the number of  $\delta t$ -measurement records in a  $\Delta t$ -time interval  $[t_j, t_j + \Delta t]$ . Once  $I_{t_j}$  and  $\phi_{t_j}$  are obtained, we then compute the coarse-grained state evolution following

$$|\psi_{X_{t_j}}(t_j + \Delta t)\rangle = \frac{\hat{M}_A(X_{t_j})|\psi(t_j)\rangle}{\sqrt{\rho_A(X_t)}} \quad (48)$$

for  $A \in \{I, R, W, \Phi, \Psi\}$  and  $X_{t_j} \in \{I_{t_j}, \phi_{t_j}\}$ . For the fixed total time  $T = 10^4\delta t$ , we obtain  $N = T/\Delta t = 100$  coarse-grained states per trajectory for each method. We illustrate an example for our simulation results in Fig. 2 for a qubit  $z$ -measurement example (Case 1).

For each of the special cases, we then generate an ensemble of quantum trajectories with  $R = 5000$  realizations and analyze the trace squared-errors (TrSEs) compared to the true trajectories, which is  $\sigma_{A;k}^2(t_j) = 2(1 - |\langle\psi_{A;k}(t_j)|\psi_{T;k}(t_j)\rangle|^2)$ . Here,  $|\psi_{A;k}(t_j)\rangle$  denotes the quantum state generated by the map  $\hat{M}_A$ , and  $|\psi_{T;k}(t_j)\rangle$  is the corresponding true state.

For better visualization, we further compute the time-average TrSEs over  $N$  time steps for a trajectory, which is defined as

$$\sigma_{A;k}^2 = \frac{1}{N} \sum_{j=1}^N \sigma_{A;k}^2(t_j). \quad (49)$$

The distributions of  $\sigma_{A;k}^2$  are presented as histograms in Fig. 3. We then average  $\sigma_{A;k}^2$  over the ensemble  $R$  realizations to obtain the MTrSE,

$$\bar{\sigma}_A^2 = \frac{1}{R} \sum_{k=1}^R \sigma_{A;k}^2 \quad (50)$$

where  $\bar{\sigma}_A^2 = \bar{\sigma}_{I_t}^2(\hat{\psi}_{A;I_t})$  defined in Eq. (15).

Finally, since the TrAE was also analyzed in the preceding section and analytically in Ref. [24], we compute  $D_{A;k}(t_j) = \sqrt{1 - |\langle \psi_{A;k}(t_j) | \psi_{R;k}(t_j) \rangle|^2}$  and additionally compute the *mean trace-absolute error* (MTrAE), defined as

$$\bar{D}_A = \frac{1}{R} \sum_{k=1}^R \frac{1}{N} \sum_{j=1}^N D_{A;k}(t_j). \quad (51)$$

This quantity enables a direct and consistent comparison between our numerical error analysis and the existing analytical results reported in Ref. [24].

## B. Numerical results

Let us analyze the numerical results of the time-average TrSEs shown as histograms for five examples and all methods in Fig. 3. The Example 1 in the first column, we demonstrate Case 1, where  $\hat{c} = \sqrt{\gamma/2}\hat{\sigma}_z$  with  $\hat{c}^2 \propto \hat{1}$ . In this example, as predicted by Eqs. (40), the map  $\hat{M}_I$  becomes comparable to  $\hat{M}_R$  and  $\hat{M}_W$ , with the MTrSEs in the order of  $O(10^{-7})$ .

To connect with our analytical results in Ref. [24], we compute the MTrAEs. For  $N$  time steps, we find that the average trace distance follows

$$\bar{D}_A = \frac{2}{3} \sqrt{N} D_A, \quad (52)$$

where the full derivation of Eq. (52) is provided in Appendix C. Here,  $D_A$  is the *one-time-step* average distance of trajectories generated by the map  $\hat{M}_A$  compared to the *exactly solvable* maps over the *exact probability distribution* [24]. The values of  $D_A$  were derived in Table II of Ref. [24]. In this example, the analytical distances are

$$\begin{aligned} D_I &= 0.2585(\gamma\Delta t)^{3/2}, \\ D_R &= 0.1551(\gamma\Delta t)^{3/2}, \\ D_W &= 0.0699(\gamma\Delta t)^{3/2}. \end{aligned}$$

Substituting these values into Eq. (52) with  $\gamma\Delta t = 10^{-2}$  and  $N = 100$ , we find good agreement with the histogram data, yielding  $\bar{D}_A = O[(\gamma\Delta t)^{3/2}] = O(10^{-3})$  for  $A \in \{I, R, W\}$ , with small discrepancies due to the finite ensemble size in the numerical simulations.

Crucially, since  $[\hat{c}, \hat{c}^\dagger] = 0$  in this example, we observe that  $\hat{M}_{\text{R}}$  generates more accurate trajectories than the other methods, including  $\hat{M}_\Phi$ , which is aligned with the predictions in Eqs. (44). We note that, although the pure state  $|\psi_{\text{R}}\rangle$  exhibits errors with  $\bar{\sigma}_{\text{R};k}^2 = O[(\gamma\Delta t)^{(5/2)^2}] = O(10^{-10})$  due to the truncation of  $\hat{M}_{\text{R}}$ , no such error is expected for the corresponding  $\rho_{\text{R}}$  in this case.

Moving to the second column of Fig. 3, we present Example 2, corresponding to the qubit fluorescence measurement with  $\hat{c} = \sqrt{\gamma}\hat{\sigma}_-$ . As expected, we find that  $\bar{\sigma}_I^2 = \bar{\sigma}_R^2$  and  $\bar{\sigma}_W^2 = \bar{\sigma}_{\text{R}}^2$ , with these four maps producing MTrSEs of order  $O[(\gamma\Delta t)^3] = O(10^{-6})$ . The map  $\hat{M}_\Phi$  now produces trajectories with the smallest MTrSEs, while  $\hat{M}_{\text{R}}$  is no longer the most accurate method as  $\hat{c}$  is not normal. Note that, in this example,  $D_A$  was also derived in Ref. [24], reported in Table II, where

$$\begin{aligned} D_I &= D_R = 0.1152(\gamma\Delta t)^{3/2}, \\ D_W &= 0.0576(\gamma\Delta t)^{3/2}. \end{aligned}$$

We find that the corresponding numerical results  $\bar{D}_A$  for  $A \in \{I, R, W\}$  as displayed in the plots in the second column lead to an agreement with the analytical results  $D_A$  via Eq. (52).

Example 3 is shown in the third column, where  $\hat{c} = \sqrt{\gamma}\hat{S}_-$  for a spin-1 system. In this case, the Itô map generates the largest errors, with  $\bar{\sigma}_I^2 = O[(\gamma\Delta t)^2] = O(10^{-4})$ , while the errors associated with  $\hat{M}_A$  for  $A \in \{R, W, \text{R}\}$  now exhibit the same scaling as  $O[(\Delta t)^3] = O(10^{-6})$  with different prefactors. In this case, the Itô map is no longer comparable with  $\hat{M}_R$  and  $\hat{M}_W$  since  $\hat{c}^2$  is not proportional to  $\hat{1}$ , unlike in Example 1. Notably, we see that  $\bar{\sigma}_W^2 \simeq \bar{\sigma}_{\text{R}}^2$ , both scaling as  $O(10^{-6})$ , in agreement with the prediction of Eq. (42b). This example is consistent with the behavior expected for Case 3.

Example 4, shown in the fourth column of Fig. 3, corresponds to Case 4. Here, the operator  $\hat{c}$  is normal, satisfying  $[\hat{c}, \hat{c}^\dagger] = 0$ , and we take  $\hat{c} = \sqrt{\gamma/2}\hat{S}_z$  for a spin-1 system. As expected, the robinet method again produces the smallest MTrSEs. However, the  $\hat{M}_\Phi$  still outperforms the other maps with scaling  $\bar{\sigma}_\Phi^2 = O[(\Delta t)^4] = O(10^{-8})$ , while  $\bar{\sigma}_W^2, \bar{\sigma}_R^2 = O[(\Delta t)^3] = O(10^{-6})$  and  $\bar{\sigma}_I^2 = O[(\Delta t)^2] = O(10^{-4})$ .

Finally, Example 5 is shown in the fifth column of Fig. 3, where we take  $\hat{c} = \sqrt{\gamma}\hat{L}_-$  for a spin-3/2 system. This example reflects Case 5. The map  $\hat{M}_\Phi$  produces the smallest MTrSEs, scaling as  $\bar{\sigma}_\Phi^2 = O[(\Delta t)^4] = O(10^{-8})$ , while the other maps,  $\hat{M}_R$ ,  $\hat{M}_W$ , and  $\hat{M}_{\text{R}}$ , exhibit MTrSEs scaling as  $O[(\gamma\Delta t)^3] = O(10^{-6})$ , with different numerical prefactors, and  $\bar{\sigma}_I^2 = O[(\Delta t)^2] = O(10^{-4})$ .

## V. CONCLUSION

We have analyzed the errors in quantum trajectory simulations arising from finite experimental time resolution, which lead to quantum evolution conditioned only on time-binned measurement records  $I_t$ . Existing higher-order approaches—including the Itô expansion, the maps of Rouchon–Ralph [21] and Wonglakhon *et al.* [24], and the robinet

method [25]—have deviations of order  $O[(\Delta t)^{3/2}]$  from the fully conditioned state. This is so even though the robinet map  $\mathcal{K}_{\hat{c}}$  is optimal given the time-binned record  $I_t$ , because it is fundamentally limited by information lost in the time-binning process itself.

This led us to derive what we call the  $\Phi$ -map, by returning again to the system–bath Hamiltonian formalism. This map incorporates a single additional record variable,  $\phi_t$ , yet achieves trajectory estimates with an error scaling of order  $(\Delta t)^2$  relative to the fully conditioned state  $\hat{\psi}_{F;\hat{y}_t}$ . Using analytically solvable solutions, we quantified the typical distances between  $\hat{\psi}_{F;\hat{y}_t}$  and the trajectories generated by existing methods for arbitrary measurement operators  $\hat{c}$ , as well as measurement operators satisfying a variety of special conditions.

Our analysis further reveals that the accuracy of  $\mathcal{K}_{\hat{c}}$  is limited by non-QND effects where  $[\hat{H}, \hat{c}] \neq 0$  or  $[\hat{c}^\dagger, \hat{c}] \neq 0$ . These non-commutativities give rise to evolution terms involving the additional record  $\phi_t$  that cannot be neglected for higher-order accuracy. In contrast, for QND measurements where  $\hat{c}$  is normal and satisfies  $[\hat{H}, \hat{c}] = 0$ , we find that the variable  $\phi_t$  vanishes from the evolution, and the robinet method becomes exact. We verified this analytic finding, and other special cases, with numerical simulations for a variety of finite-dimensional systems.

Overall, the  $\Phi$ -map provides the highest accuracy presently available for general quantum trajectory estimation while requiring only a doubling of record variables, from  $I_t$  alone to

$\{I_t, \phi_t\}$ . While  $I_t$  is readily accessible in standard experiments, extracting  $\phi_t$  would presumably require a dedicated electronic processing scheme. Designing such schemes remains an open and promising direction for future research.

## ACKNOWLEDGEMENT

This research was supported by the Australian Research Council Centre of Excellence Program [grant number CE170100012] and the Program Management Unit for Human Resources and Institutional Development, Research and Innovation (Thailand) [grant number B05F630108].

## DATA AVAILABILITY

The data that support the findings of this article are openly available [32].

## Appendix A: Nearly exact map derivation

Following Eq. (21), we construct the nearly exact map by keeping the deterministic terms to  $O[(dt)^2]$  and stochastic terms to  $O[(dt)^{3/2}]$ . Hence, we obtain all possible terms as follows:

$$\begin{aligned} \hat{M}_{3/2} = & \hat{1} + \hat{c}Y_t\Delta t - \left[ \frac{1}{2}\hat{c}^\dagger\hat{c} - \frac{1}{2}\hat{c}^2(Y_t^2\Delta t - 1) + i\hat{H} \right] \Delta t \\ & + \lim_{m \rightarrow \infty} \left\{ -\frac{1}{2}\hat{c}\hat{c}^\dagger\hat{c} \sum_{j=0}^{m-1} y_j dt \left( jdt + \frac{1}{3}dt \right) - \frac{1}{2}\hat{c}^\dagger\hat{c}^2 \sum_{j=0}^{m-1} y_j dt \left[ (m-j)dt + \frac{2}{3}dt \right] - i\hat{c}\hat{H} \sum_{j=0}^{m-1} y_j dt \left( jdt + \frac{1}{2}dt \right) \right. \\ & - i\hat{H}\hat{c} \sum_{j=0}^{m-1} y_j dt \left[ (m-j)dt + \frac{1}{2}dt \right] + \hat{c}^3 \left[ \sum_{j=0}^{m-1} y_j dt \sum_{k=0}^{j-1} \frac{1}{2}(y_k^2 dt - 1)dt + \sum_{j=0}^{m-1} \frac{1}{2}(y_j^2 dt - 1)dt \sum_{k=0}^{j-1} y_k dt \right. \\ & \left. \left. + \sum_{j=0}^{m-1} y_j dt \sum_{k=0}^{j-1} y_k dt \sum_{\ell=0}^{k-1} y_\ell dt + \sum_{j=0}^{m-1} \frac{1}{6}(y_j^3 dt - 3y_j)dt^2 \right] \right\}. \quad (A1) \end{aligned}$$

For the first line in RHS of Eq. (A1), the first three terms are trivial and have been shown in Ref. [24].

For the second line and the first term of the third line of Eq. (A1), these terms are the exchange of  $y_s\hat{c}dt \times \hat{R}$ ,  $\hat{1} \times A y_s \hat{c} \hat{R} dt^2$  and  $\hat{1} \times A y_s \hat{R} \hat{c}^\dagger dt^2$  with  $\hat{R} = -i\hat{H}dt - \frac{1}{2}\hat{c}^\dagger\hat{c}dt$  for a relevant coefficient  $A$ . Here, we can express the relevant

four forms of the infinite sums as follows:

$$\begin{aligned} \lim_{m \rightarrow \infty} \sum_{j=0}^{m-1} y_j dt (jdt + Adt) &= \int_t^{t+\Delta t} ds y_s [\Delta t - (s-t)] \\ &= \frac{1}{2}\Delta t^2 Y_t + Z_t, \quad (A2a) \end{aligned}$$

$$\begin{aligned} \lim_{m \rightarrow \infty} \sum_{j=0}^{m-1} y_j dt [(m-j)dt + Adt] &= \int_t^{t+\Delta t} ds y_s [\Delta t - (s-t)] \\ &= \frac{1}{2}\Delta t^2 Y_t - Z_t, \quad (A2b) \end{aligned}$$

which are in terms of  $Y_t$  and  $Z_t$  records as defined in the main text. Thus, we have  $\frac{1}{2}Y_t\Delta t^2\{\hat{c}, \hat{R}\} + Z_t[\hat{c}, \hat{R}] = -\frac{1}{2}Y_t\Delta t^2\{\hat{c}, i\hat{H} + \frac{1}{2}\hat{c}^\dagger\hat{c}\} - Z_t[\hat{c}, i\hat{H} + \frac{1}{2}\hat{c}^\dagger\hat{c}]$ . We note that there

are errors in Appendix C of Ref. [24]. The prefactors for  $\hat{c}\hat{c}^\dagger\hat{c}$  and  $\hat{c}^\dagger\hat{c}^2$  in Eqs. (C7) and (C8) should follow Eqs. (A2) above. However, this does not affect the results in Ref. [24] as they only focus on the ensemble average evolution to  $(\Delta t)^2$ , while the contribution from  $Z_t$  appears in  $(\Delta t)^3$ .

The rest of the terms in Eq. (A1) are proportional to  $\hat{c}^3$ , which are a result of four possible exchanges: (a)  $y_s\hat{c}dt \times \frac{1}{2}(y_s^2dt - 1)\hat{c}^2dt$ , (b)  $\frac{1}{2}(y_s^2dt - 1)\hat{c}^2dt \times y_s\hat{c}dt$ , (c)  $y_s\hat{c}dt \times y_s\hat{c}dt \times y_s\hat{c}dt$ , and (d)  $\hat{1} \times \frac{1}{6}(y_s^3dt - 3y_s)dt^2\hat{c}^3$ .

For the exchange (a), we can write the relevant form:

$$\sum_{j=0}^{m-1} y_j dt \sum_{k=0}^{j-1} \frac{1}{2}(y_k^2 dt - 1) dt = \frac{1}{2} \sum_{j>k=0}^{m-1} y_j dt (y_k^2 dt - 1) dt. \quad (\text{A3})$$

Likewise the exchange (b), we write:

$$\sum_{j=0}^{m-1} \frac{1}{2}(y_j^2 dt - 1) dt \sum_{k=0}^{j-1} y_k dt = \frac{1}{2} \sum_{j>k=0}^{m-1} (y_j^2 dt - 1) dt y_k dt. \quad (\text{A4})$$

Here, we combine Eq. (A3) and Eq. (A4), which is simplified

to:

$$\begin{aligned} & \frac{1}{2} \sum_{j>k=0}^{m-1} y_j dt (y_k^2 dt - 1) dt + \frac{1}{2} \sum_{j>k=0}^{m-1} (y_j^2 dt - 1) dt y_k dt \\ &= \sum_{j=0}^{m-1} y_j dt \sum_{k=0}^{m-1} \frac{1}{2}(y_k^2 dt - 1) dt - \sum_{j=0}^{m-1} \frac{1}{2} y_j (y_j^2 dt - 1) dt^2 \\ &= \frac{1}{2} \Delta t Y_t \sum_{j=0}^{m-1} (y_j^2 dt - 1) dt - \frac{1}{2} \sum_{j=0}^{m-1} y_j (y_j^2 dt - 1) dt^2. \end{aligned} \quad (\text{A5})$$

For the exchange (c), we express:

$$\sum_{j=0}^{m-1} y_j dt \sum_{k=0}^{j-1} y_k dt \sum_{\ell=0}^{k-1} y_\ell dt = \sum_{j>k>\ell=0}^{m-1} y_j y_k y_\ell dt^3. \quad (\text{A6})$$

By using the fact that

$$\begin{aligned} \Delta t^3 Y_t^3 &= \sum_{j,k,\ell=0}^{m-1} y_j y_k y_\ell dt^3 \\ &= \sum_{j=0}^{m-1} y_j^3 dt^3 + 3 \sum_{j \neq k=0}^{m-1} y_j^2 y_k dt^3 + 6 \sum_{j>k>\ell=0}^{m-1} y_j y_k y_\ell dt^3, \end{aligned}$$

we can be reformulated Eq. (A6) as

$$\begin{aligned} \sum_{j>k>\ell=0}^{m-1} y_j y_k y_\ell dt^3 &= \frac{1}{6} \left[ \Delta t^3 Y_t^3 - \sum_{j=0}^{m-1} y_j^3 dt^3 - 3 \sum_{j \neq k=0}^{m-1} y_j^2 y_k dt^3 \right] = \frac{1}{6} \Delta t^3 Y_t^3 - \frac{1}{6} \sum_{j=0}^{m-1} y_j^3 dt^3 - \frac{1}{2} \left( \sum_{j,k=0}^{m-1} y_j^2 y_k dt^3 - \sum_{j=0}^{m-1} y_j^3 dt^3 \right) \\ &= \frac{1}{6} \Delta t^3 Y_t^3 - \frac{1}{6} \sum_{j=0}^{m-1} y_j^3 dt^3 - \frac{1}{2} \left( \Delta t Y_t \sum_{j=0}^{m-1} y_j^2 dt^2 - \sum_{j=0}^{m-1} y_j^3 dt^3 \right). \end{aligned} \quad (\text{A7})$$

Lastly, for the exchange (d), we have

$$\sum_{j=0}^{m-1} \frac{1}{6}(y_j^3 dt - 3y_j) dt^2. \quad (\text{A8})$$

Thus, combining Eqs. (A5), (A7) and (A8), we find the terms that is proportional to  $\hat{c}^3$  as

$$\begin{aligned} & \frac{1}{2} \Delta t Y_t \sum_{j=0}^{m-1} (y_j^2 dt - 1) dt - \frac{1}{2} \sum_{j=0}^{m-1} y_j (y_j^2 dt - 1) dt^2 + \frac{1}{6} \Delta t^3 Y_t^3 - \frac{1}{6} \sum_{j=0}^{m-1} y_j^3 dt^3 \\ & \quad - \frac{1}{2} \left( \Delta t Y_t \sum_{j=0}^{m-1} y_j^2 dt^2 - \sum_{j=0}^{m-1} y_j^3 dt^3 \right) + \sum_{j=0}^{m-1} \frac{1}{6}(y_j^3 dt - 3y_j) dt^2 = \frac{1}{6} \Delta t^3 Y_t^3 - \frac{1}{2} \Delta t^2 Y_t. \end{aligned} \quad (\text{A9})$$

Finally, the coefficient of  $\hat{c}^3$  reads:  $\frac{1}{6}(\Delta t Y_t^3 - 3Y_t)\Delta t^2\hat{c}^3$  and obtain the closed form as

$$\begin{aligned} \hat{M}_{3/2}(Y_t, Z_t) &= \hat{1} - \frac{1}{2}\hat{c}^\dagger\hat{c}\Delta t + \hat{c}\Delta t Y_t + \frac{1}{2}\hat{c}^2[Y_t^2\Delta t^2 - \Delta t] \\ &+ \frac{1}{6}\Delta t^2\hat{c}^3(Y_t^3\Delta t - 3Y_t) - \frac{1}{2}\{\hat{c}, i\hat{H} + \frac{1}{2}\hat{c}^\dagger\hat{c}\}\Delta t^2 Y_t \\ &- Z_t [\hat{c}, i\hat{H} + \frac{1}{2}\hat{c}^\dagger\hat{c}] + \frac{1}{2}\left[\left(\frac{1}{2}\hat{c}^\dagger\hat{c}\right)^2 - \hat{H}^2\right]\Delta t^2, \end{aligned} \quad (\text{A10})$$

where the variable  $Z_t$  was first introduced in Ref. [24], defined as

$$Z_t \equiv \int_t^{t+\Delta t} ds y_s \left[ s - \left( t + \frac{\Delta t}{2} \right) \right]. \quad (\text{A11})$$

The variable  $Z_t$  also has a Gaussian ostensible probability dis-

tribution, given by

$$\varphi_{\text{ost}}(Z_t) = \sqrt{\frac{6}{\pi \Delta t^3}} \exp(-6Z_t^2/\Delta t^3). \quad (\text{A12})$$

It has been shown that  $Y_t$  and  $Z_t$  are statistically independent, i.e.,  $\text{E}[Y_t Z_t]_{y_s} = 0$ , where we have used the ensemble average notation:  $\text{E}[\bullet]_{y_t} \equiv \int_{-\infty}^{\infty} dy_t \varphi_{\text{ost}}(y_t) \bullet$ . Given the independence of  $Y_t$  and  $Z_t$ , the Kraus form of the nearly exact map reads  $\hat{K}_{3/2}(Y_t, Z_t) = \sqrt{\varphi_{\text{ost}}(Y_t) \varphi_{\text{ost}}(Z_t)} \hat{M}_{3/2}(Y_t, Z_t)$ .

## Appendix B: Relevant operators for special cases

For the spin-1/2 (qubit) case, we use the Pauli operators defined as

$$\hat{\sigma}_x = \begin{pmatrix} 0 & 1 \\ 1 & 0 \end{pmatrix}, \quad \hat{\sigma}_y = \begin{pmatrix} 0 & -i \\ i & 0 \end{pmatrix}, \quad \hat{\sigma}_z = \begin{pmatrix} 1 & 0 \\ 0 & -1 \end{pmatrix}, \quad (\text{B1})$$

with the initial state

$$|+x\rangle = \frac{1}{\sqrt{2}} \begin{pmatrix} 1 \\ 1 \end{pmatrix}. \quad (\text{B2})$$

For the spin-1 system, we use the following operators

$$\hat{S}_x = \begin{pmatrix} 0 & 1 & 0 \\ 1 & 0 & 1 \\ 0 & 1 & 0 \end{pmatrix}, \quad \hat{S}_y = \begin{pmatrix} 0 & -i & 0 \\ i & 0 & -i \\ 0 & i & 0 \end{pmatrix}, \quad \hat{S}_z = \begin{pmatrix} 1 & 0 & 0 \\ 0 & 0 & 0 \\ 0 & 0 & -1 \end{pmatrix}, \quad (\text{B3})$$

with the initial state

$$|+x\rangle_1 = \frac{1}{2} \begin{pmatrix} 1 \\ \sqrt{2} \\ 1 \end{pmatrix}. \quad (\text{B4})$$

Lastly, we use the following for the spin-3/2 system lowering operator, given by

$$\hat{L}_- = \frac{1}{2} \begin{pmatrix} 0 & 0 & 0 & 0 \\ \sqrt{3} & 0 & 0 & 0 \\ 0 & 2 & 0 & 0 \\ 0 & 0 & \sqrt{3} & 0 \end{pmatrix}, \quad (\text{B5})$$

and the initial state,

$$|+x\rangle_{3/2} = \frac{1}{\sqrt{8}} \begin{pmatrix} 1 \\ \sqrt{3} \\ \sqrt{3} \\ 1 \end{pmatrix}. \quad (\text{B6})$$

## Appendix C: Derivation for the overall average trace distance

The goal of this derivation is to show the relationship between the accumulating  $N$  time steps trace distance with a single time step trace distance from the known results in Ref [24].

Let us first consider a Gaussian random variable  $Q$ , featuring the probability distribution  $\varphi_Q$  with  $\mu_Q$  mean and  $\sigma_Q^2$  variance. Here, we define the absolute distance between the random variable  $q$  and its mean for one time step as  $D_q \equiv |q - \mu_Q|$ . The distance average is given by

$$\text{E}[D_q]_Q = \sqrt{\frac{2}{\pi}} \sigma, \quad (\text{C1})$$

and we can re-express the variance via  $\sigma^2 = \frac{\pi}{2} \text{E}^2[D_q]_Q$ . Assuming the variance accumulates linearly over time, we can express the variance after  $k$ -th time step as

$$k\sigma^2 = \frac{k\pi}{2} \text{E}^2[D_q]_Q. \quad (\text{C2})$$

Hence, we obtain the relation:  $\sqrt{(\frac{2}{\pi}k)\sigma} = \sqrt{k} \text{E}[D_q]_Q$ , for the absolute distance distance at  $k$ -th time-steps. We can compute the average overall distance after  $K$  time steps, given by

$$\bar{D} = \frac{1}{K} \sum_{k=0}^K \sqrt{k} \text{E}[D_q]_Q. \quad (\text{C3})$$

For a large number  $K$ , we can replace the summation to an integral as

$$\bar{D} = \frac{\text{E}[D_q]_Q}{K} \int_0^K dk \sqrt{k} = \frac{2}{3} \sqrt{K} \text{E}[D_q]_Q. \quad (\text{C4})$$

As we already have the analytical results for  $\text{E}[D_q]_Q \rightarrow D_A$  from Ref. [24] (for the qubit cases) and in our simulation we use  $K \rightarrow N$ , we have the overall average trace distance after  $N$  time steps are given by

$$\bar{D}_A = \frac{2}{3} \sqrt{N} D_A. \quad (\text{C5})$$

---

[1] H. J. Carmichael, *An Open Systems Approach to Quantum Optics* (Springer, Berlin, 1993).  
[2] A. Barchielli, Quantum Optics: Journal of the European Optical Society Part B **2**, 423 (1990).  
[3] H. M. Wiseman and G. J. Milburn, Phys. Rev. A **47**, 642 (1993).  
[4] H. M. Wiseman and G. J. Milburn, Phys. Rev. A **47**, 1652 (1993).  
[5] M. B. Plenio and P. L. Knight, Rev. Mod. Phys. **70**, 101 (1998).  
[6] K. W. Murch, S. J. Weber, C. Macklin, and I. Siddiqi, Nature **502**, 211 (2013).

[7] S. J. Weber, A. Chantasri, J. Dressel, A. N. Jordan, K. W. Murch, and I. Siddiqi, *Nature* **511**, 570 (2014).

[8] A. Chantasri, M. E. Kimchi-Schwartz, N. Roch, I. Siddiqi, and A. N. Jordan, *Phys. Rev. X* **6**, 041052 (2016).

[9] S. Hacohen-Gourgy, L. S. Martin, E. Flurin, V. V. Ramasesh, K. B. Whaley, and I. Siddiqi, *Nature* **538**, 491 (2016).

[10] B. Q. Baragiola and J. Combes, *Phys. Rev. A* **96**, 023819 (2017).

[11] Z. K. Minev, S. O. Mundhada, S. Shankar, P. Reinhold, R. Gutiérrez-Jáuregui, R. J. Schoelkopf, M. Mirrahimi, H. J. Carmichael, and M. H. Devoret, *Nature* **570**, 200 (2019).

[12] D. A. Ivanov, T. Y. Ivanova, S. F. Caballero-Benitez, and I. B. Mekhov, *Phys. Rev. Lett.* **124**, 010603 (2020).

[13] L. S. Martin, W. P. Livingston, S. Hacohen-Gourgy, H. M. Wiseman, and I. Siddiqi, *Nature Physics* **16**, 1046 (2020).

[14] J. Steinmetz, D. Das, I. Siddiqi, and A. N. Jordan, *Phys. Rev. A* **105**, 052229 (2022).

[15] P. Guilmin, P. Rouchon, and A. Tilloy, *IFAC-PapersOnLine* **56**, 5164 (2023), 22nd IFAC World Congress.

[16] V. P. Belavkin, *Rep. Math. Phys.* **43**, A405 (1999).

[17] H. M. Wiseman and G. J. Milburn, *Quantum Measurement and Control* (Cambridge University Press, 2009).

[18] K. Jacobs, *Stochastic Processes for Physicists: Understanding Noisy Systems* (Cambridge University Press, 2010).

[19] E. B. Davies, *Communications in Mathematical Physics* **15**, 277 (1969).

[20] C. W. Gardiner, *Handbook of Stochastic Methods: For Physics, Chemistry and the Natural Science* (Springer-Verlag, Berlin, 1985).

[21] P. Rouchon and J. F. Ralph, *Phys. Rev. A* **91**, 012118 (2015).

[22] I. Guevara and H. M. Wiseman, *Phys. Rev. A* **102**, 052217 (2020).

[23] P. Rouchon, *Annual Reviews in Control* **54**, 252 (2022).

[24] N. Wonglakhon, H. M. Wiseman, and A. Chantasri, *Phys. Rev. A* **110**, 062207 (2024).

[25] P. Guilmin, P. Rouchon, and A. Tilloy, “Time-averaged continuous quantum measurement,” (2025), arXiv:2505.20382 [quant-ph].

[26] The subscript we use on  $\rho_{\text{faucet}}$  was chosen because Ref. [25] call their state the *robinet* [faucet or tap] state, a pun on the Franglais term  $\rho\text{-binné}$  [binned  $\rho$ ].

[27] C.-I. Philippe, *Measurement back action and feedback in superconducting circuits.*, Ph.D. thesis, Ecole Normale Supérieure (ENS) (2015).

[28] G. Milstein, *Numerical Integration of Stochastic Differential Equations* (Springer, 1995).

[29] G. Lindblad, *Communications in Mathematical Physics* **48**, 119 (1976).

[30] L. Li, M. J. Hall, and H. M. Wiseman, *Physics Reports* **759**, 1 (2018), concepts of quantum non-Markovianity: A hierarchy.

[31] M. M. Wilde, “Preface to the second edition,” in *Quantum Information Theory* (Cambridge University Press, 2017) p. xi–xii.

[32] N. Wonglakhon, “natwonglakhon/high-order-quantum-trajectory-simulation: High-order-quantum-trajectory-simulation,” (2026).